Supplementary Material:
Effects of oscillating gas-phase flow on an evaporating multicomponent droplet
S. Majee, A. Saha, S. Basu

1. Strength of Marangoni Flow due to temperature and concentration gradient:

Here, we discuss the possible role of Marangoni convection in our study. This can be achieved by comparing the flow velocity due to Marangoni stress (U_M) and aerodynamic shear stress (U_s) at the droplet surface. The Marangoni flow velocity can be expressed as $U_M = \Delta\sigma/\mu_l$. Here, $\Delta\sigma$ is the change in surface tension across the interface due to temperature and concentration gradients, which can be elaborated as, $\Delta\sigma = \left[\left(\frac{\partial\sigma}{\partial T}\right)_{Y_w} dT + \left(\frac{\partial\sigma}{\partial Y_w}\right)_T dY_w\right]$. Here, Y_w is the mass fraction of water in the liquid phase at the droplet surface. Thus, the Marangoni flow velocity can be expressed as,

$$U_M = \left[\left(\frac{\partial\sigma}{\partial T}\right)_{Y_w} dT + \left(\frac{\partial\sigma}{\partial Y_w}\right)_T dY_w\right]/\mu_l. \tag{1.1}$$

Based on the correlation presented by Nayar *et al.* (2014), we find that within the temperature and concentration range of our study, the surface tension gradients are expected to be in the order $(\partial\sigma/\partial T)_{Y_w} \approx -10^{-4} N/m/^o C$ and $(\partial\sigma/\partial Y_w)_T \approx -10^{-4} N/m/(w/w\%)$. From contour plots of T and Y (figure in manuscript), we expect the scales for variation in them to be in the order of $dT \approx 0.01^o C$ and $dY_w \approx 0.01(w/w\%)$, respectively for most of the droplet lifetime. Substituting these scales in Eq. 1.1, along with the value of liquid viscosity ($\mu_l \approx 10^{-3}$Pa-s), we find the velocity scale of Marangoni flow to be $U_M \approx 10^{-3}$m/s.

As we described in the paper, the aerodynamic shear-driven flow velocity at the droplet surface is

$$U_s = (1/32)(U_g - U_p)(\mu_g/\mu_l) Re_p C_F. \tag{1.2}$$

Here, μ_g is the gas phase dynamic viscosity ($\approx 10^{-5}$Pa-s), and C_F is the skin friction coefficient for an evaporating sphere calculated using the correlation given by $C_F = 12.69 Re_p^{-2/3}/(1 + B_M)$. The Reynolds number is $Re_p = (2\rho_g|U_p - U_g|r_s)\mu_g$. Since the gas phase velocity is in the order of 1 m/s, and $(1 + B_M) \approx 1$, we estimate the shear-driven velocity scale to $U_s \approx 10^{-2}$m/s, which is an order of magnitude higher than U_M.

Thus, in this study, Marangoni flow can be considered weak. If the gas phase temperature is significantly higher than the initial droplet temperature (for example, evaporation and combustion of fuel droplets injected in engines of gas turbines), the dT is expected to be significantly higher, and as such, Marangoni flow will be comparable to the shear driven flow at the droplet interface, as shown by Niazmand *et al.* (1994); Dwyer *et al.* (1996, 1998).

2. Grid independence study:

We have performed a grid convergence study using various grid sizes in the liquid phase. It is to be noted that the liquid phase inside the droplet was solved using a polar $(r - \theta)$ coordinate system, where both the dimensions (r and θ) were discretized using an equal number of grid points. In Fig. 1, we compared the diameter regression rate for three different grid sizes. We notice that all droplet size history is very close for all three grid sizes. Careful observation also reflects that, beyond the 20x20 grid size, the difference in results becomes insignificant. Thus, we used a 20x20 grid size for the rest of the study.

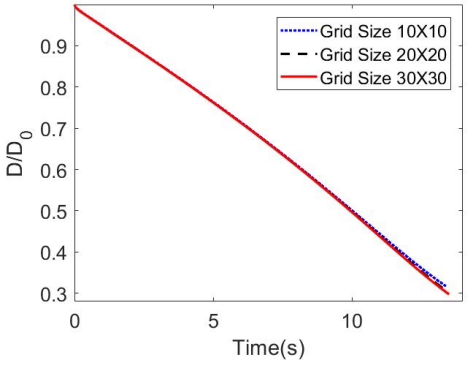

Figure 1: Diameter regression history for three different grid sizes.

Property	**Values**
Density of water, ρ_w	980 kg/m^3
Density of salt, ρ_s	2160 kg/m^3
Density of air, ρ_g	0.9918 kg/m^3
Specific heat of water, $C_{p,w}$	4.18×10^3 J/KgK
Specific heat of salt, $C_{p,s}$	0.86×10^3 J/KgK
Specific heat of air, $C_{p,g}$	1.007×10^3 J/KgK
Dynamic viscosity of gas phase, μ_g	18×10^{-6} Pa-s
Dynamic viscosity of liquid phase, μ_l	7.94×10^{-4} Pa-s
Thermal conductivity of liquid phase, k_l	0.6 W/mK
Thermal conductivity of gas phase, k_g	26.62×10^{-3} W/mK
Binary diffusivity (water vapor in air), D_v	22.5×10^{-6} m^2/s
Binary diffusivity (salt in water), $D_{v,Za}$	1×10^{-9} m^2/s
Latent heat of evaporation for water, $h_{f,g}$	2439×10^3 J/Kg
Vapor pressure of water, $P_{sat}(T)$	$P_{sat}(bar) = 10^{A-B/(T(K)+C)}$, where A=4.6543, B=1435.264, C=-64.848

Table 1: Property values.

3. Physical properties

In table 1, we have listed the property values used for this study.

4. Effect of added mass and Basset history force on drag force

The drag force on a spherical particle or droplet can include various effects. The simplified form used for this study (equations 2.1 and 2.3 in the manuscript) only considers the *steady*

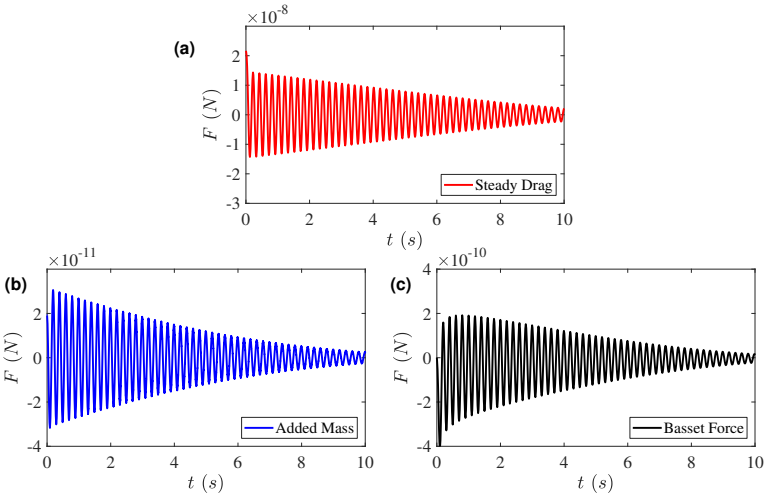

Figure 2: Comparison of three different drag forces. (a) steady drag is considered for our study. (b) added mass effect, and (c) Basset history force were neglected in our study. We can see the latter two are significantly smaller than the steady-state drag.

drag forces. However, it has been shown that the *added mass effect* and the *Basset history force* can also contribute to the drag forces on a particle or droplet in an accelerating or decelerating flow (Odar & Hamilton 1964; Berlemont *et al.* 1990; Aggarwal & Peng 1995). The contribution from the *added mass effect* can be evaluated by

$$F_{am} = -\frac{4\pi}{3} r_s^3 \rho_g \frac{d}{dt}\left(U_p - U_g\right) + \frac{4\pi}{3} r_s^3 \rho_g \frac{D}{Dt}\left(U_g\right), \tag{4.1}$$

where D/Dt is the material derivative, and C_a is the drag coefficient due to added mass effect, which is close to 1 (Aggarwal & Peng 1995). On the other hand, the contribution from the *Basset history force* can be expressed as

$$F_{bf} = -\pi r_s^2 C_h \sqrt{\frac{\rho_g \mu_g}{\pi}} \int_0^t \frac{\frac{d(U_p - U_g)}{dt}}{\sqrt{t - t'}} dt', \tag{4.2}$$

where t' is a dummy variable for integration and C_h is the drag coefficient due to Basset force, which is about 2.3 (Aggarwal & Peng 1995). The details about these forces can be found in literature (Odar & Hamilton 1964; Berlemont *et al.* 1990; Aggarwal & Peng 1995).

In the context of our simulation, we have evaluated the three effects on drag and their time histories, shown in Fig. 2. The steady-state drag, considered for the simulation, is almost 3 and 2 orders of magnitude larger than the added mass effect and the Basset history force, respectively. We neglected the latter two terms for evaluating drag force. This assumption also allows obtaining a closed-form expression for the scaling analysis.

REFERENCES

Aggarwal, SK & Peng, F 1995 A Review of Droplet Dynamics and Vaporization Modeling for Engineering Calculations. *Journal of Engineering for Gas Turbines and Power* **117** (3), 453–461.

Berlemont, Alain, Desjonqueres, Philippe & Gouesbet, Gérard 1990 Particle lagrangian simulation in turbulent flows. *International Journal of Multiphase Flow* **16** (1), 19–34.

Dwyer, HA, Aharon, I, Shaw, BD & Niamand, H 1996 Surface tension influences on methanol droplet vaproiation in the presence of water. In *Symposium (International) on Combustion*, , vol. 26, pp. 1613–1619. Elsevier.

Dwyer, HA, Shaw, BD & Niazmand, H 1998 Droplet/flame interactions including surface tension influences. In *Symposium (international) on combustion*, , vol. 27, pp. 1951–1957. Elsevier.

Nayar, Kishor Govind, Panchanathan, Divya, McKinley, GH & Lienhard, JH 2014 Surface tension of seawater. *Journal of Physical and Chemical Reference Data* **43** (4), 043103.

Niazmand, H, Shaw, BD, Dwyer, HA & Aharon, I 1994 Effects of marangoni convection on transient droplet evaporation. *Combustion science and technology* **103** (1-6), 219–233.

Odar, Fuat & Hamilton, Wallis S 1964 Forces on a sphere accelerating in a viscous fluid. *Journal of fluid mechanics* **18** (2), 302–314.